

ADVANCEMENTS IN MATERIALS FOR THREE-DIMENSIONAL PRINTING OF MOLDS AND CORES

J. Thiel , S. Ravi, and N. Bryant

Metal Casting Center, University of Northern Iowa, Cedar Falls, IA, USA

Copyright © 2016 American Foundry Society
DOI 10.1007/s40962-016-0082-y

Abstract

Three-dimensional printing of sand molds and cores is changing the way castings are produced. During the last 5 years major advances in equipment have allowed metalcasters to realize casting designs at faster speeds than ever before. The elimination of tooling for mold and cores assemblies has allowed the industry new flexibility in design optimization, reduced labor, increased dimensional accuracy, and eliminated some defects associated with core assembly. While the equipment has been advancing, the materials used for printing have been very limited. The University of Northern Iowa has conducted new research into increasing the number of materials available for printing. These materials include regionally available resins, aggregates, and additives. These new materials have the ability to reduce the cost of printing and increase

the number of applications while improving the casting quality. Veining defects in heavy iron or steel castings once prevalent on printed sand molds can be eliminated with engineered sand additives. Solidification rate and penetration defects can be addressed with specialty molding aggregates. This research has allowed the users of printed sand molds and cores to realize the potential of their sand printers and improve the quality of the castings they produced. The paper will detail the experiences with regionally available materials and compare their properties and performance with conventionally supplied materials.

Keywords: additive manufacturing, molding materials, 3D printing, bonded sands

Introduction

Three-dimensional printing of cores and molds has come of age. Metalcasters are now able to drastically reduce lead times for pattern tooling while taking advantage of design freedom never before envisioned. Additive manufacturing for metal castings, AM4MC represents one of the most significant developments in metalcasting technology in years.

The basic process introduced over 20 years ago has gained significant ground over the last 2 years. The technology once used exclusively for prototype low quantity is now being used for production cores and molds. The ability to produce very complex core assemblies has replaced a significant amount of manual labor not just in the core room but also in casting finishing operations. Single-piece cores are replacing core assemblies that were manually glued in fixtures and mudded to seal joints.

Ninety percent of cores produced in North America utilize the phenolic urethane no-bake of cold box resin system. This robust process provides long working times and bench life along with good mechanical strength and compatibility with additives.

Almost all of the current three-dimensional sand printers utilize the furan resin system catalyzed by sulfonic acid. Furan resins were very popular during the period from 1970 to 1985 in the foundry industry because of their high productivity and strength levels but price fluctuations and uncertain availability moved the foundry industry toward urethane and phenolic resins. The furan system is still used in foundry applications worldwide and has achieved a fair amount of market stability. It is available in several forms from several North America resin suppliers. It develops high tensile strengths while providing excellent shakeout and sand release from internal passageways.

While research continues on printing urethane or phenolic resins, furan systems remain the predominant systems in AM4MC applications. Recent testing has shown that although the furan sands are acid-catalyzed, thermal reclamation effectively neutralizes the acidity of the sand making it compatible with phenolic urethane systems.

Equipment Technology

The equipment technology for AM4MC has been advancing at a tremendous rate. Developed by MIT researchers in the late 1980s it was licensed by three companies based in Germany. Zcorp had developed a resin system based on sodium silicate but ceased its sale and support of the printers in 2013. The remaining company split into what are the two largest manufacturers of sand mold printers. The first-generation sand printers introduced in the early 2000s were already reaching the end of their service life and considered slow and inflexible. The second-generation machines introduced in the late 2000s were two to three times as fast and twice as large. New equipment introduced in 2015 are touted to be twice as large again and four times as productive as the second-generation equipment. North America suppliers have responded to the German-made equipment with robotic arm printers promising to lower the cost of printed sand at a fraction of the price of larger units. The newest company to enter the market promises to combine very fast print times, low cost of equipment with freedom to use conventional sands and resins. This has the potential to lower the cost of printing sand to a point easily justifiable by even small foundries.

The printing system works by creating image files from individual slices of the solid objects. These image files are then printed in order of successive layers of sand to recreate the solid objects. The print head is rastered across the print area depositing droplets of resin as ink would be printed on an image.

The sand setup screen allows changes to the printer settings such as sand layer thickness, X axis resolution, speed of the print head, bidirectional offset, and percentage of new sand, previously activated sand and additive percentage. The universities additive feeder was modified to allow for higher additive addition rates than originally designed for. The recipe screen is shown in Figure 1.

Reclaimed sand is proportioned to utilize excess unbonded material that has been vacuumed from the work area. New sand and pre-activated sand are fed from two double-stacked hoppers capable of holding around 3000 lbs each. Filling of the sand containers is possible during printing operations. The sand is pulled from the hoppers by the use of vacuum transfer feeders to smaller storage hoppers above the printer and mixing chamber. The mixing sequence includes a new sand addition, a catalyst addition based on new sand only,

pre-activated reclaimed sand addition, and additives before being discharged into the re-coater.

As each layer is printed, the work area is lowered to compensate for the next layer. The re-coater spreads the sand evenly over the entire work area while compacting the sand. The resin then is selectively printed on to the areas defined by the image slice files. The process is repeated up to 2700 times until the work area is filled.

After all of the layers have been printed, the sand container is removed from the printer and catalyzed but unbound sand is removed by vacuuming. The sand is screened and returned to the reclaimed sand hopper.

Testing Methodology

Research over the last 10 years has demonstrated that much if not all of the original materials developed for AM4MC can be replaced with regionally available materials. This ability gives the metalcaster greater control over the process and subsequent quality of the molds and cores.

The spreading and printing of bonded sand requires a specific set of characteristics that are outside conventional sand testing. Printing sand requires that the sand be spread at a constant height and density across an area as large as two meters. In order for this to occur the sand must easily flow with agitation and remain stable at rest. It also must be able to be compacted without deformation and have excellent permeability. To evaluate various potential molding aggregates for the sand printing process, the University of Northern Iowa developed a set of tests that evaluated mechanical properties, physical properties, and performance properties and ranked the results in a surface plot. The results of the testing were used as a guide for opportunities to substitute for currently used aggregates.

Extensive research was conducted on the general characterizations of different aggregates. This characterization included mechanical, physical, and chemical properties of both unbonded and furan binder system bonded aggregates. It must be noted that the bonded samples made with the furan binder system were made conventionally. Table 1 shows the different aggregates tested.

Mechanical Properties

Mechanical properties included bulk density as defined by the AFS procedure 1130-00-S, tapped density per 1131-00-S, surface area per AFS 1108-00-S, grain shape or coefficient of angularity per AFS 1126-00-S, base permeability per AFS 1119-00-S, and nonstandard tests including angle of repose, material flow rate, and penetration force. The penetration force was determined by measuring the resistance of a 1" (25 mm) plate being pushed into a container

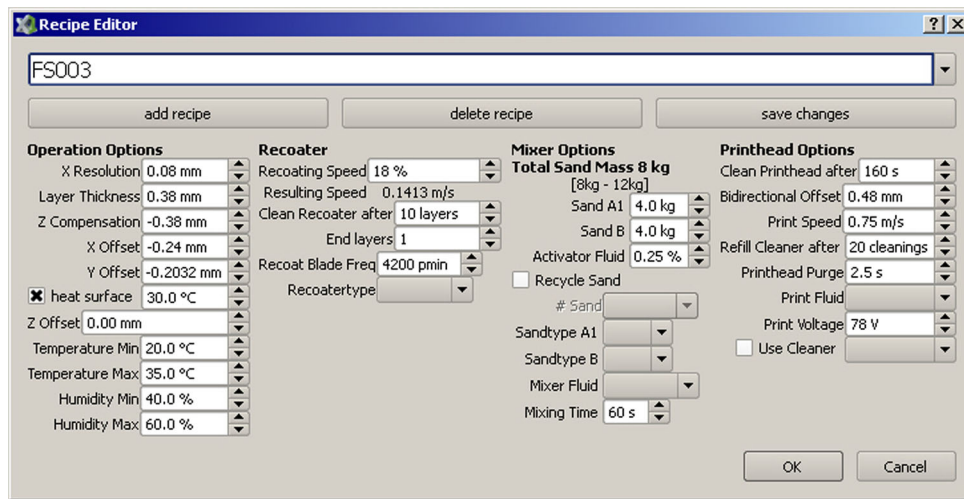


Figure 1. Recipe editor screen for ExOne S-Max printer.

Table 1. Aggregates Tested

Sample	Aggregate
1	Silica M4000
2	Carbo Accucast ID50-K
3	Carbo Accucast LD70
4	ORC chromite
5	Ceramsite
6	Cerabeads
7	Fused silica (crushed)
8	Incast 70
9	Incast 8-
10	Manley "Acti Sand"
11	Carbo 100/140

Table 2. Untapped and Tapped Bulk Density Results for all Aggregates

Aggregate	Bulk density (g/cc)	Tapped density (g/cc)
Silica M4000	1.554	1.769
Carbo Accucast ID50-K	1.819	2.070
Carbo Accucast LD70	1.424	1.694
ORC chromite	2.694	3.015
Ceramsite	1.839	2.007
Cerabeads	1.422	1.723
Fused silica (crushed)	0.989	1.256
Incast 70	1.516	1.673
Incast 80	1.445	1.620
Manley "Acti Sand"	1.438	1.623
Carbo 100/140	1.41	1.510

of the material. The maximum force and penetration distance at the maximum force were recorded for all samples along with the sand displacement in pounds per inch.

Mechanical Properties Results

The untapped and tapped bulk density results are shown in Table 2. With the exception of the specialty aggregates such as the ceramics and mullites, it can be observed that the untapped density of the silica sand samples is typically in the range of 1.4–1.6 g/cc. However, looking at the tapped density results, it can be observed that certain aggregates are arranged better upon tapping when compared to others. This largely depends on the grain shape factor of the aggregate. Silica M4000 has a tapped bulk density of 1.769 g/cc, which is the highest among the silica sand aggregates. Carbo 100/140 aggregate has a tapped density of 1.510 g/cc. The other silica sand aggregates are observed to range between 1.6 and 1.7 g/cc.

The AFS grain fineness number (GFN) and surface area for the aggregates are shown in Table 3. With the exception of the ceramics and Incast 70, which have a lower AFS-GFN, the other aggregates have a GFN of 80–100. Silica M4000, Carbo Accucast LD70, ceramsite, and fused silica have a higher surface area when compared to the other samples. This will result in these aggregates requiring higher binder content to achieve similar strength levels. Fused silica, in particular, was measured to have a surface area of 437.9 cm²/g, which is high for a molding aggregate.

The flow rate and base permeability results for the aggregates are shown in Table 4. Flow rate is an important property for three-dimensional printing as the aggregate needs to have an optimum flow rate in order to fill the sand bed. With the exception of fused silica, it can be observed that most aggregates display similar flow rates. ORC chromite and ceramsite were observed to have a higher flow rate when compared to the other aggregates. Permeability of sand is crucial in venting the gases due to binder

Table 3. AFS-GFN and Surface Area Results for all Aggregates

Aggregate	AFS-GFN	Surface area (cm ² /g)
Silica M4000	81.90	270.685
Carbo Accucast ID50-K	54.87	142.00
Carbo Accucast LD70	64.56	252.694
ORC chromite	89.30	94.172
Ceramsite	92.26	238.775
Cerabeads	66.47	183.101
Fused silica (crushed)	96.80	437.918
Incast 70	66.515	183.832
Incast 80	79.821	184.983
Manley "Acti Sand"	102.493	265.561
Carbo 100/140	80.415	152.545

Table 4. Flow Rate and Base Permeability Results for all Aggregates

Aggregate	Flow rate (g/s)	Base permeability
Silica M4000	4.69	37.38
Carbo Accucast ID50-K	5.22	137.33
Carbo Accucast LD70	4.02	99.00
ORC chromite	8.52	49.00
Ceramsite	6.22	51.33
Cerabeads	3.84	62.33
Fused silica (crushed)	2.50	35.00
Incast 70	4.32	51.67
Incast 80	4.36	52.00
Manley "Acti Sand"	4.20	42.67
Carbo 100/140	4.19	70.00

decomposition from the mold. An aggregate with lower permeability will often have gas porosity in the castings. However, if the permeability is too high, metal penetration defects will occur in the casting. It can be seen that Silica M4000 and fused silica have lower base permeability when compared to the other samples. The ID50-K and LD70 aggregates show higher permeability. The other samples have a base permeability of ~50–70.

Physical Properties

Physical properties tested included linear expansion, surface viscosity, sinter point, specific heat capacity, heat-dependent density acid demand value, and pH.

Physical Property Results

Table 5 shows the pH and acid demand value (ADV) results for the aggregates. For the furan binder system, an

Table 5. pH and ADV Results for all Aggregates

Aggregate	PH	ADV
Silica M4000	7.55	0.27
Carbo Accucast ID50-K	7.33	0.92
Carbo Accucast LD70	7.04	−0.45
ORC chromite	6.63	0.08
Ceramsite	8.16	0.55
Cerabeads	9.38	2.65
Fused silica (crushed)	6.76	0.10
Incast 70	7.41	−0.43
Incast 80	7.53	1.47
Manley "Acti Sand"	7.58	0.13
Carbo 100/140	6.64	−0.067

aggregate with a pH on the basic side or a higher ADV will not bond easily, due to a higher acid catalyst requirement. It can be seen that most aggregates tested have a pH between 6.5 and 8.15. The one exception, Cerabeads, was measured to have a higher pH of 9.38. Cerabeads also had a higher ADV of 2.65 when compared to the other samples.

The thermal expansion results are shown in Figure 2. Firstly, it can be observed that all specialty aggregates, including the ceramics and chromite, display a very low expansion when compared to the silica sand samples. All the silica sand samples are observed to go through the alpha–beta phase transition at 573 °C (1063 °F). It can be observed that the fused silica aggregate displays the higher peak expansion at this phase transition.

Following this phase transition, the samples contract steadily leading to the cristobalite phase transition at higher temperature, which occurs at different temperatures for the samples and depends on the purity of the sand sample. Table 6 shows the sinter temperature and peak surface viscosity for all samples.

Specific heat capacity and temperature-dependent density tests were run for all samples. Figure 3 shows the specific heat capacity result for Silica M4000. A steady decrease in specific heat capacity was observed from room temperature to ~900 °C after which the specific heat capacity was observed to increase to 1600 °C.

Figure 4 shows the density result for Silica M4000. The density is observed to decrease from room temperature leading to the alpha–beta phase transition. After this transition, a steady increase in density can be observed up to the cristobalite phase transition. After the cristobalite phase transition, a rapid decrease in density can be observed.

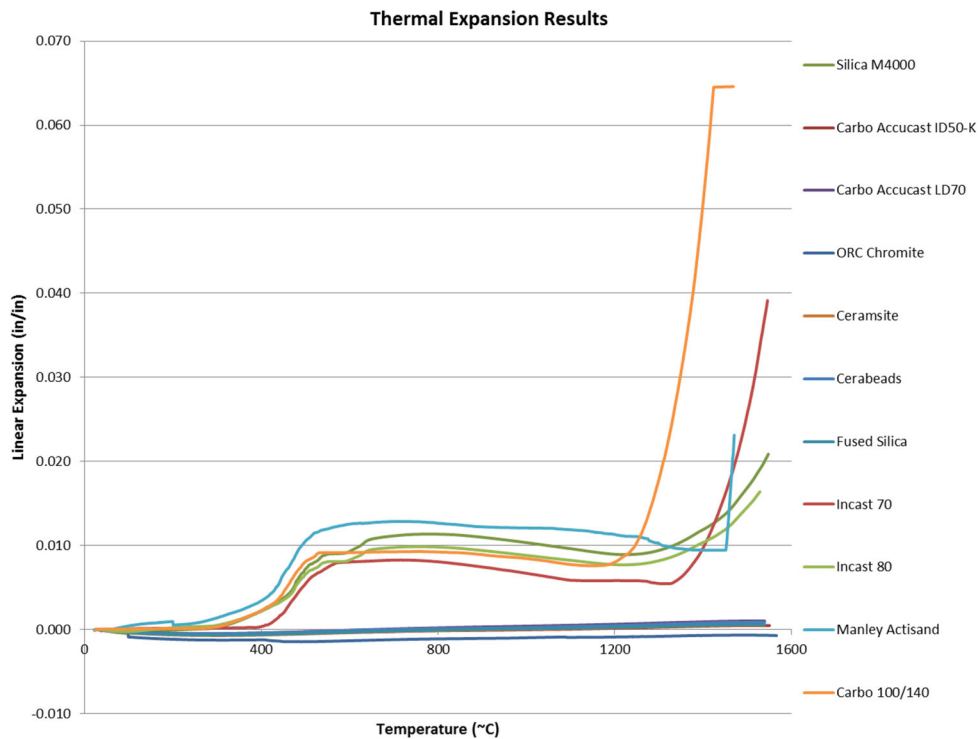


Figure 2. Thermal expansion results for all aggregates.

Table 6. Sinter Temperature and Peak Surface Viscosity Results

Aggregate	Sinter temperature (C)	Peak surface viscosity (Pa.s)
Silica M4000	1276	1.011×10^8
Carbo Accucast ID50-K	1550	6.125×10^9
Carbo Accucast LD70	1550	2.563×10^9
ORC chromite	1525	4.482×10^9
Ceramsite	1550	3.489×10^9
Cerabeads	1550	8.201×10^9
Fused silica (crushed)	1550	2.411×10^9
Incast 70	1297	1.463×10^8
Incast 80	1293	2.643×10^8
Manley "Acti Sand"	1420.7	2.92×10^8
Carbo 100/140	1209	1.04×10^8

Performance Properties

Performance properties consisted of specific tensile strength, hot strength, loss on ignition (LOI), and the graded results of step-cone testing in both gray iron and steel alloys.

Performance Property Results

The room-temperature tensile strength results at 24 h are shown in Table 7. The binder content used for the samples

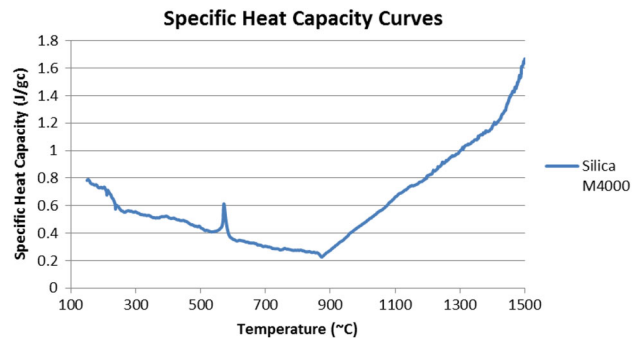


Figure 3. Silica M4000 specific heat capacity result.

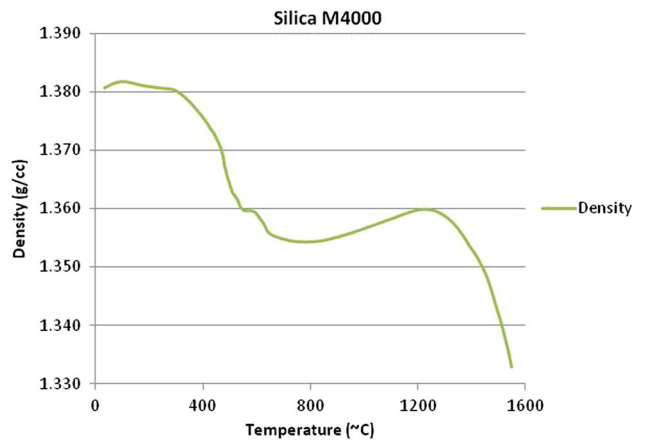


Figure 4. Silica M4000 temperature-dependent density result.

Table 7. Binder Content and Tensile Strength at 24 Hours

Aggregate	Tensile strength (psi)	Binder content (%)
Silica M4000	141	1
Carbo Accucast ID50-K	124.8	2.5
Carbo Accucast LD70	118.50	2
ORC chromite	148.2	1.25
Ceramsite	107.3	1.5
Cerabeads	103.2	2.5
Fused silica (crushed)	28.2	1
Incast 70	53.6	1
Incast 80	73.7	1
Manley "Acti Sand"	62.3	1
Carbo 100/140	134.4	1

is displayed along with the strengths. It can be seen that the specialty aggregates, especially the ceramics, needed a higher binder content to obtain good tensile strength results. All the silica sand samples were bonded with 1 % binder content. However, it was observed that Carbo 100/140 and Silica M4000 displayed higher tensile strengths. Fused silica, Incast 70, Incast 80 and Manley Acti Sand showed lower tensile strengths with 1 % binder.

The LOI results for the samples is shown in Table 7. Loss on ignition tests was run on unbonded samples. It can be observed that three samples were measured to have negative LOI values. It should be noted that these three samples are specialty aggregates and the increase in sample weight at the end of the test is due to high-temperature reactions. Cerabeads was observed to have a very high LOI content, for an unbonded sample. The silica sand samples show typical values and range from 0.02 to 0.12 % LOI.

The hot strength results for the bonded aggregates are shown in Table 8. These results include the yield strength and the modulus. It can be observed that ORC chromite shows a high yield strength and modulus when compared to the other samples. The modulus of the silica sand samples typically ranged in between 100,000 and 200,000 psi, with the exception of Silica M4000 and Manley Acti Sand.

Step-cone test castings were poured with all bonded aggregates to evaluate castings for veining and penetration defects, surface finish, and gas bubble defects. Castings were poured using a standard class 30 gray iron and weldable cast B composition (WCB) steel. Figure 5 shows the iron step-cone casting for Silica M4000. Veining defects can be observed in the casting, which is typical of a high-purity silica sand iron casting.

Table 8. Loss on Ignition Results for all Aggregates

Aggregate	Loss on ignition (%)
Silica M4000	0.060
Carbo Accucast ID50-K	-0.016
Carbo Accucast LD70	0.073
ORC chromite	-0.617
Ceramsite	-0.113
Cerabeads	1.130
Fused silica (crushed)	0.021
Incast 70	0.100
Incast 80	0.106
Manley "Acti Sand"	0.106
Carbo 100/140	0.120

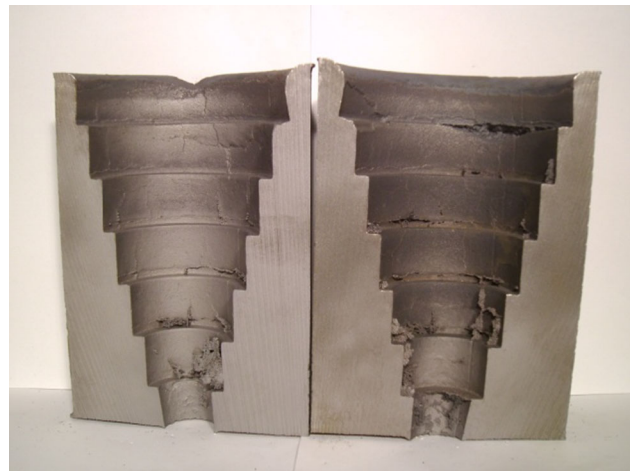


Figure 5. Silica M4000 gray iron step-cone casting.

Combined Results Surface Plot

The mechanical, physical, and performance properties results obtained for the aggregates were used in an algorithm to develop a surface plot displaying all three categories for each aggregate. The formulas were developed by placing results that expressed preferred high values in the numerator and preferred low values in the denominator. Constants were used to adjust the range of the results to similar numerical values. Using the methodology, results with high and low preferred values would increase the score of the material.

Mechanical, physical, and performance properties were evaluated by the using the following formulas.

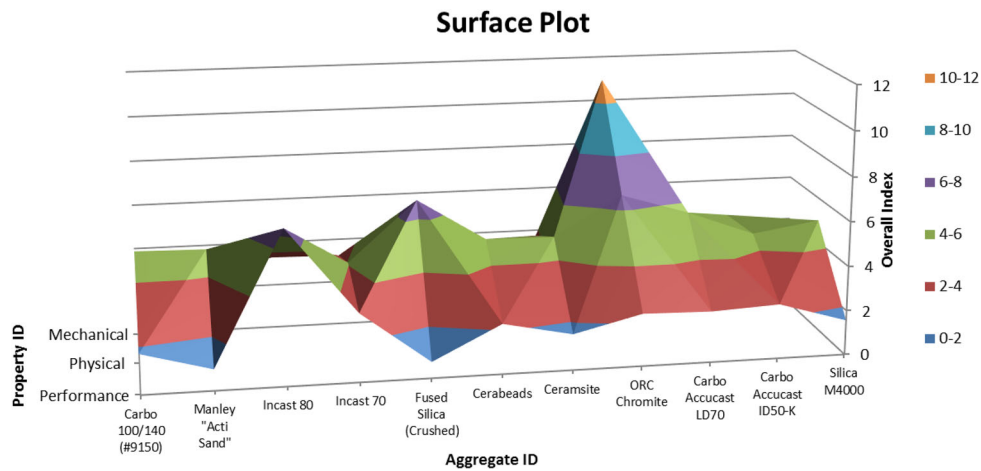


Figure 6. Surface plot of combined results.

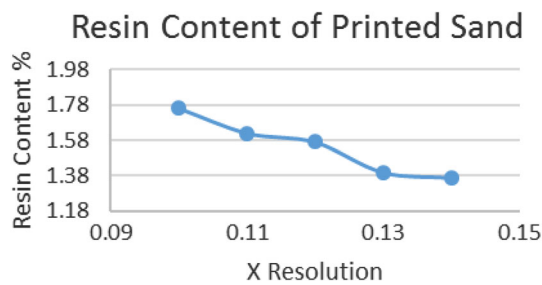


Figure 7. Resin content as a function of X resolution.

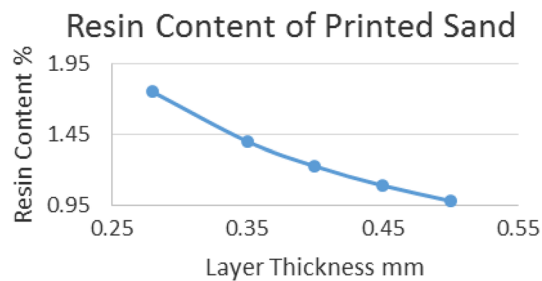


Figure 8. Resin content as a function of printed layer thickness.

Mechanical Properties

$$\frac{(\text{sand displacement} + \text{bulk density} + \text{tapped density} + \text{flow rate})}{(\text{surface area} + (100 - \text{GFN}) + \text{grain shape} + \text{angle of repose})} \times 100.$$

Eqn. 1

Physical Properties

$$\frac{(50000 - ((\text{sinter point} + \text{surface viscosity}) / \text{peak linear expansion} + \text{acid demand value} + (-7 + \text{pH}))/1000000))}{100000}.$$

Eqn. 2

Performance Properties

$$\frac{(\text{specific strength} + \text{hot yield strength})}{(\text{LOI} + ((\text{steel veining score} + \text{steel penetration score} + (\text{steel surface finish score} \times 0.1) + \text{steel gas bubble score} + \text{iron penetration score} + (\text{iron surface finish score} \times 0.1) + \text{iron gas bubble score}) \times 0.5))}.$$

Eqn. 3

The surface plot is shown in Figure 6. On the Y axis, a higher Y score depicts better performance of the aggregate. It can be observed that ORC chromite showed good performance in physical and mechanical properties but showed poor performance characteristics. Incast 80 silica sand was observed to have good performance characteristics when compared to other aggregates and comparable physical and mechanical properties.

Replacement Material Considerations

When replacing materials used in the equipment it is important to identify the characteristics of the material by physical and mechanical test methodologies. Two of these critical tests include screen distribution and bonded strength testing.

The research to date has included silica sands with GFN's ranging from 45 to 90 GFN, zircon sands from 85 to 105 GFN, and ceramic sands from 50 to 70 GFN. Before discussing the results it is important to understand the effect of various printer settings on the results of the testing.

The operator has control over much of the settings of the printer allowing for optimization for individual materials. The resin content applied to the sand is controlled by three printer settings. The first is the X resolution setting. This controls the spacing between the pulses of the print head. The closer the pulses of resin are together, the higher the resin content will be. This is shown in Figure 7.

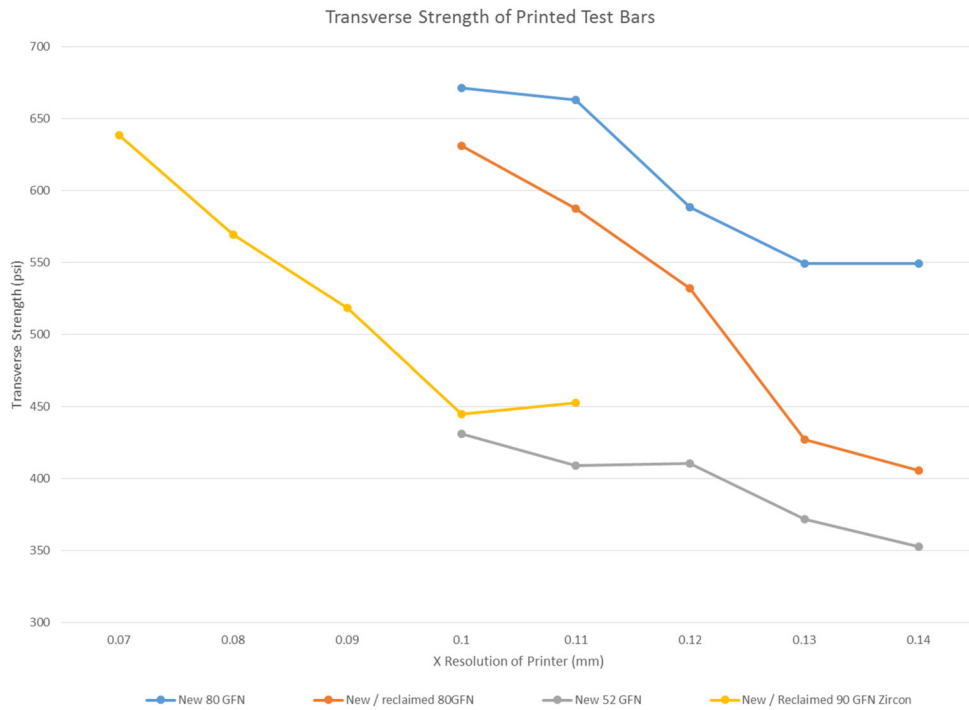


Figure 9. Strength of printed sand relative to the resin content along the x axis.

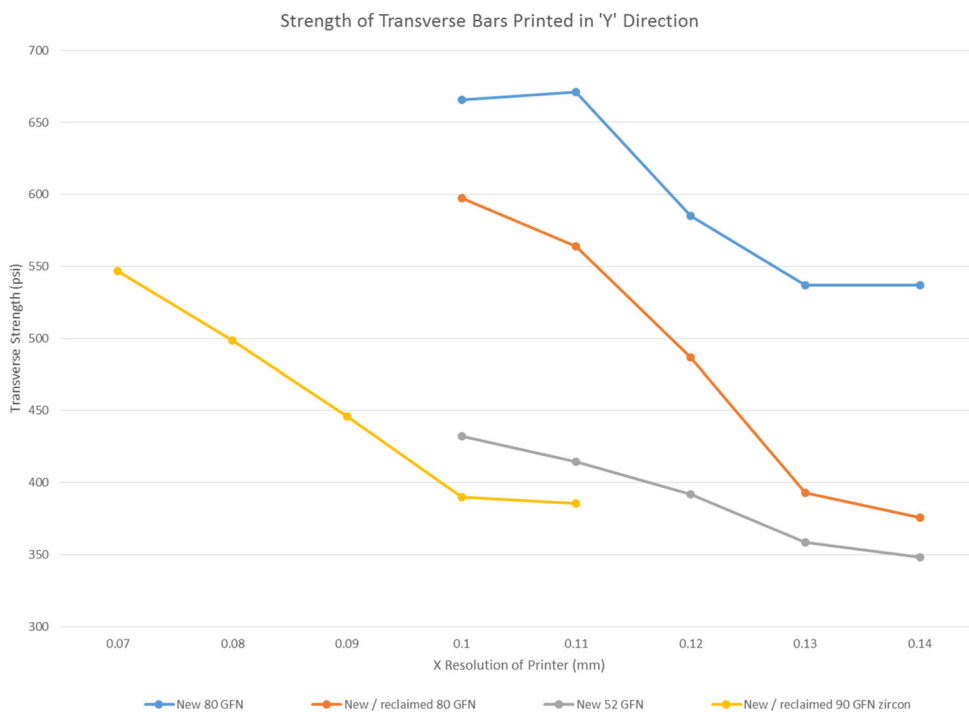


Figure 10. Strength of printed sand relative to the resin content along the y axis.

The Y resolution is considered adjustable but fixed. The second method of adjusting resin content is through varying the layer thickness, Z dimension. Typical Z print layer thickness is between 0.2 and 0.5 mm. Sands containing less fine material, <140 mesh lend themselves to thicker printed layers. As the fine material is increased the surface area

also increases along with the resin path to previous layers. Figure 8 illustrates the resin content as a function of printed layer thickness.

The voltage supplied to the print head is considered a third variable controlling the amount of resin released with

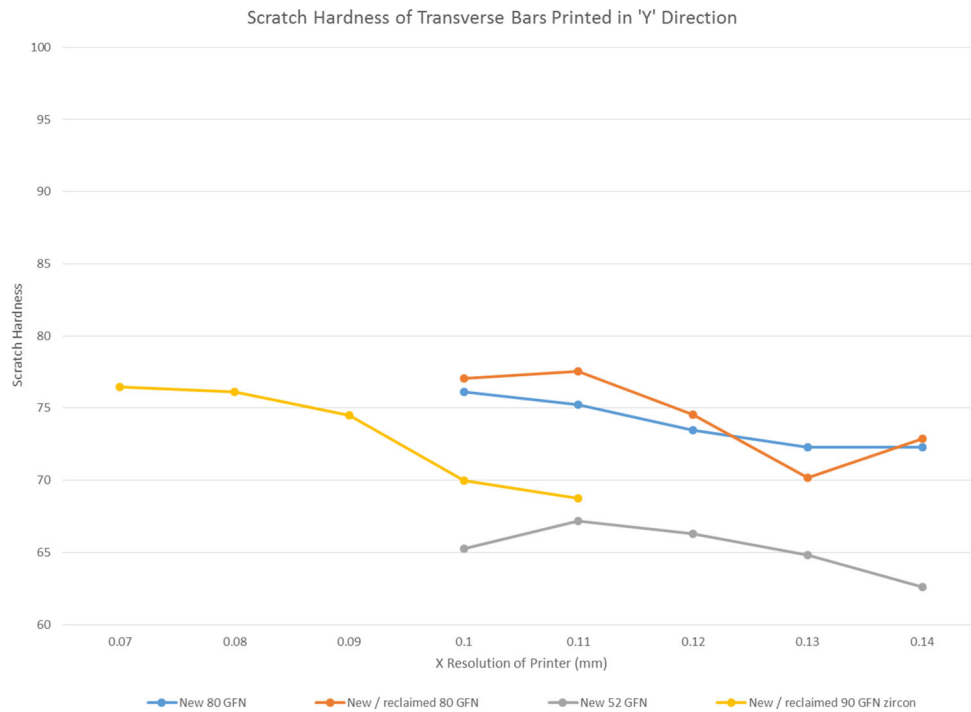


Figure 11. Scratch hardness of printed sand relative to the resin content along the x axis.

individual pulses. Since increasing the print head voltage may adversely affect the life of the print head, this was not studied.

Other printer settings such as the speed of the re-coater (sand spreader) have some minimal effect on the mechanical properties of the printed sand but work within a narrow window without detrimental effects. The speed at which the resin is deposited does not appear to have any effect on the quality of the printed sand.

Screen Distribution

The grain fineness as defined by AFS procedure 1106-12-S represents an estimate of average sieve size of a sand sample. Results of several sands tested during the research are listed in Tables 1, 2, and 3.

Transverse Strength

The resin content is directly proportional to the strength of the printed sand. Other factors including surface area and aggregate type also influence the strength of the printed sand. Figure 9 illustrates the strength of various aggregates relative to the X resolution and resin content. It was noted that the orientation of the test bars within the print area in relation to the X and Y axis of the machine had an influence in the transverse strength. Bars printed in the Y direction had a transverse strength approximately 10 % lower than those printed in the X direction as shown in Figure 10.

Table 9. Hot Strength Results for all Aggregates

Aggregate	Yield strength (psi)	Modulus (psi)
Silica M4000	7.439	43490.8
Carbo Accucast ID50-K	30.121	176838.9
Carbo Accucast LD70	22.673	147534.5
ORC chromite	45.587	339062.4
Ceramsite	9.438	106375.8
Cerabeads	21.274	126817.9
Fused silica (crushed)	4.849	39398.1
Incast 70	15.635	169472.4
Incast 80	12.519	205931.9
Manley "Acti Sand"	10.369	43377.3
Carbo 100/140	17.553	163732.7

Scratch Hardness

Scratch hardness defined by AFS 3318-10-S procedure tests the surface hardness of the printed core or mold. The test gives an indication of the resistance of the printed sand to rubbing or surface marking. Results of various sands are listed in Figure 11. Sands listed with the term reclaimed refer to the use of pre-activated sand that was previously used but not bonded in the sand printing process (Tables 9, 10, 11, 12).

Table 10. Silica (M4000) Screen Distribution

Sieve size	Cumulative weight	Retained on screen	% Retained	Multiplier	Product
20	0.000	0.000	0.00	0.10	0.0000
30	0.000	0.000	0.00	0.20	0.0000
40	0.020	0.020	0.04	0.30	0.0119
50	0.053	0.033	0.07	0.40	0.0261
70	0.187	0.134	0.27	0.50	0.1326
100	31.477	31.290	61.93	0.70	43.3500
140	49.784	18.307	36.23	1.00	36.2328
200	50.483	0.699	1.38	1.40	1.9368
270	50.494	0.011	0.02	2.00	0.0435
Pan	50.500	0.006	0.01	3.00	0.0356
Total	50.53	50.50	99.95	GFN	81.77

Table 11. Silica (46 GFN) Screen Distribution

Sieve size	Cumulative weight	Retained on screen	% Retained	Multiplier	Product
20	0.000	0.000	0.00	0.10	0.0000
30	0.019	0.019	0.04	0.20	0.0076
40	6.680	6.661	13.27	0.30	3.9801
50	29.366	22.686	45.18	0.40	18.0740
70	44.227	14.861	29.60	0.50	14.7997
100	48.841	4.614	9.19	0.70	6.4330
140	49.759	0.918	1.83	1.00	1.8284
200	50.163	0.404	0.80	1.40	1.1265
270	50.193	0.030	0.06	2.00	0.1195
Pan	50.196	0.003	0.01	3.00	0.0179
Total	50.207	50.20	99.98	GFN	46.39

Table 12. Silica (80 GFN) Screen Distribution

Sieve size	Cumulative weight	Retained on screen	% Retained	Multiplier	Product
20	0.000	0.000	0.00	0.10	0.0000
30	0.000	0.000	0.00	0.20	0.0000
40	0.007	0.007	0.01	0.30	0.0039
50	0.029	0.022	0.04	0.40	0.0165
70	7.900	7.871	14.76	0.50	7.3798
100	36.875	28.975	54.33	0.70	38.0335
140	50.917	14.042	26.33	1.00	26.3314
200	53.096	2.179	4.09	1.40	5.7204
270	53.258	0.162	0.30	2.00	0.6076
Pan	53.261	0.003	0.01	3.00	0.0169
Total	53.328	53.26	99.87	GFN	78.11

Conclusions

The measure of acceptability of printed molds often depends on the mechanical strength and resistance to damage that would change the dimensions of the printed mold or core. Although there are many other types of

bonded sand, it has been shown that the current printing equipment has the ability to print multiple materials that possess comparable mechanical properties and excellent casting results.